Beam-Riding Simulation and Diagnostics for Beamed-Energy Vehicles

Stefan Scharring[a], Hans-Albert Eckel[a], and Hans-Peter Röser[b]

[a]*Institute of Technical Physics, German Aerospace Center (DLR), Pfaffenwaldring 38 – 40, 70569 Stuttgart, Germany*
[b]*Institute of Space Systems (IRS), University of Stuttgart, Pfaffenwaldring 29, 70569 Stuttgart, Germany*

Abstract. The separation of energy source and aerospace vehicle allows for a variety of sophisticated beamed-energy propulsion concepts. Beyond the question of the technological realization of suitable high power lasers, beam-riding of the vehicle plays a crucial role for the maturity of any remotely driven laser propulsion device. Whereas usually flight stability is experimentally analyzed with respect to lateral and angular motion separately, this paper presents an analytical approach to consider as well the independency of both movements. A quasi-continuous approximation of impulse coupling yields a system of coupled differential equations describing the laser-driven motion in a two-dimensional case. A specific matrix of flight dynamics is derived yielding necessary and sufficient criteria for beam-riding stability. This approach can be applied on experimental data of any beamed-energy vehicle and shows its inherent capabilities of beam-riding and possible needs of technological assistance measures, e.g. spin-stabilization. As an example, the specific matrix of flight dynamics of a parabolic laser-thermal thruster is derived from impulse field data of recent hovering experiments. The theoretical analysis of stability criteria and simulated flight trajectories is in good accordance with the experimentally found results which had shown poor flight stability due to the specific coupling between lateral and angular motion. Furthermore, it is shown that in the mentioned case an optimization of alignment accuracy at the launch position by one order of magnitude would lead to an increase of flight time by only 1 second. The theoretical criteria for beam-riding stability are analyzed for alternative options of lightcraft configurations with respect to mass, momentum of inertia and center-of-mass position. While theoretical configurations for 2D beam-riding stability are found, alternative concepts using spin-stabilization are discussed. Model limitations with respect to full 3D dimensionality and pulsed motion are briefly illustrated.

Keywords: Beamed-energy propulsion, lightcraft, beam-riding, flight dynamics, self-stabilization, High speed analysis, Numerical approximation and analysis, CO_2 laser, Free flight experiments, Optical engineering
PACS: 05.45.Gg, 05.45.Pq, 06.60.Sx, 45.40.Gj, 47.40.Rs, 52.50.Jm, 52.77.-j, 88.85.-r

1. INTRODUCTION

Beamed energy propulsion has its origins in a revolutionary vision that firstly was introduced by Arthur Kantrowitz in 1972 [1]: The usage of high power lasers once should allow for the separation of a rocket from its energy source, being reusable and located remotely at a ground station. This would allow save a lot of energy which is only used to carry the energy carrier itself into space which is common practice in

space flight. Hence, a dramatic reduction of onboard propellant and a much better mass-to-payload ratio could be achieved.

Though this concept still seems visionary, remote energy supply has already become ordinary in Earth-bound transportation, namely in the field of electrically powered railroad. Catenary lines have provided the substitution of heavy tenders with charcoal. A comparable technological quantum leap is still missing in space flight, and beamed energy propulsion might overcome these problems.

A general issue is the mid-term availability of suitable high-power lasers meeting the requirement of 1 MW average power per kilogram payload for the launch to Low Earth Orbit [2]. Though this question remains open [3], in-space applications in a low gravity setting, e.g. sample return from an asteroid, might be feasible with already existing commercial laser sources [4]. A corresponding in-orbit demonstration experiment therefore might empower funding and research in beamed energy propulsion [5].

Nevertheless, for the confidence in the beamed energy propulsion concept, one thing is missing, i.e. the trust in the reliability of the energy link between laser source and laser-driven rocket. This is essential for any beamed energy concept, since any mission that loses this link will presumably get lost instantaneously. Therefore, with the advantages of remote energy supply the new technological risk of remote energy connection failure has to be evaluated carefully which is covered by the topic *beam-riding analysis*.

For electrically powered railroad, this problem is simply solved, since tracks guide the vehicles alongside the catenary. So, for beamed energy propulsion the question is: Does the laser beam act on the laser-propelled engine as track? In the case of misalignment of the engine to the beam: Are there restoring forces and momenta keeping the rocket on (laser) track?

In 2000, the group of L.N. Myrabo presented an impressive proof-of-principle lifting a light-weight (mass at launch: 50.6 grams) Lightcraft Technology Demonstrator (LTD) up to an altitude of 71 meters, powered by a 10 kW CO_2 laser [6]. In those experiments, beam-riding was supported by spin-stabilization. In contrast, this paper focusses on the analysis of the engine's inherent abilities of beam-riding. Spin-stabilization, which might require additional structural mass for subsequent despinning in orbit, is discussed as one possible measure if beam-riding abilities are not sufficient.

Though the LTD is commonly known as "the" lightcraft, in this paper we follow an earlier definition from Myrabo denoting lightcraft for "[…] any flight platform, airborne vehicle, or spacecraft designed for propulsion by a beam of light – be it microwave or laser. […]"[7].

2. THEORY OF MOTION COUPLING

In the following, the analytical description of the laser-induced motion is deduced from the definition of the impulse coupling coefficient c_m as a commonly known figure of merit for laser-imparted momentum vs. laser pulse energy. Usually, c_m is

used for the motion in *z*-direction which is coaxial with the laser beam propagation axis directed vertically upwards. However, experimental work has shown [8,9,10,11,12,13,14] that lateral and angular impulse components occur as well which suggest to extend this definition [14] by

$$c_{m,i} = \frac{\Delta p_i}{E_L} \approx \frac{m \cdot \Delta v_i}{E_L} \tag{1}$$

where $i = x, y, z$ denote the Cartesian coordinates of the laboratory system, yielding $c_{m,z}$ as the commonly known impulse coupling coefficient, $c_{m,x}$ and $c_{m,y}$ as lateral impulse coupling coefficients, with m as the BEP craft's mass, E_L as laser pulse energy, Δp as laser-induced impulse and Δv as laser-induced velocity increment. Similarly, the angular motion around the x-axis and y-axis, resp., can be described by the angular impulse coupling coefficients as follows

$$c_{L,i} = \frac{\Delta L_i}{E_L} \approx \frac{J_{ii} \cdot \Delta \omega_i}{E_L} \tag{2}$$

with ΔL as laser-induced impulse, Δω as laser-induced angular velocity increment, and J_{ii} as the BEP craft's moment of inertia with respect to the i-axis, assuming a rotation-symmetrical lightcraft.

A. Analytical Approximation

In the following, we focus on the BEP craft's motion in the i- z-plane, e.g. the x- z-plane, assuming for simplification that its motion perpendicular to this plane is independent from the one in plane. Then, as an approximation for higher laser pulse repetition rates,

$$\begin{pmatrix} b_i^{(m)} & b_{\vartheta,i}^{(m)} \\ b_i^{(L)} & b_{\vartheta,i}^{(L)} \end{pmatrix} \begin{pmatrix} r_i \\ \vartheta_i \end{pmatrix} \approx \begin{pmatrix} c_{m,i} \\ c_{L,i} \end{pmatrix} = \frac{1}{\bar{P}_L} \begin{pmatrix} \bar{F}_i \\ \bar{M}_i \end{pmatrix} \approx \frac{1}{\bar{P}_L} \begin{pmatrix} m \cdot \ddot{r}_i \\ J \cdot \ddot{\vartheta}_i \end{pmatrix} \tag{3}$$

holds, where the outer terms represent a linear set of differential equations that can be solved analytically. Here, the constant coefficients $b_l^{(k)}$ constitute a craft-specific matrix of flight dynamics. They describe the dependency of the lateral and angular, resp., coupling coefficient from the craft's lateral offset and inclination with respect to the beam center and orientation, resp. in a linearized approach. However, for the limited range of influence of the laser beam, this description is only valid for small values of r_i and ϑ_i. Note that in contrast to the work of [8,9,10,11], e.g., a back-driving lateral force is equivalent to a *negative* $b_i^{(m)}$. Interdependency of both motion types is provided by $b_{\vartheta,i}^{(m)}$ and $b_i^{(L)}$ if non-zero. On the right hand of the equation, the temporal

average about laser power, laser-induced force and momentum yields a link to the second derivative. Hence, with some simple substitutions, Eq. 3 can be simplified and transformed into

$$\begin{pmatrix} a & b \\ c & d \end{pmatrix} \begin{pmatrix} r_i \\ \vartheta_i \end{pmatrix} = \begin{pmatrix} \ddot{r}_i \\ \ddot{\vartheta}_i \end{pmatrix}. \tag{4}$$

B. Solutions

1. General solution

The exponential Ansatz

$$\begin{pmatrix} r(t) \\ \vartheta(t) \end{pmatrix} = \begin{pmatrix} \hat{r} \\ \hat{\vartheta} \end{pmatrix} exp(\lambda t) \tag{5}$$

with $\lambda = \kappa + i\omega, \kappa, \omega \in \mathbb{R}$ yields the characteristic equation in λ which can be solved substituting $\lambda^2 = \mu = x + iy, x, y \in \mathbb{R}$ with

$$\mu_{1,2} = \frac{a+d \pm \sqrt{(a-d)^2+4bc}}{2}. \tag{6}$$

Then, the general solution of Eq. 4 is given by [15]

$$\begin{matrix} r(t) = \sum_{i=1}^{4} r_i exp(\lambda_i t) \\ \vartheta(t) = \alpha \sum_{i=1}^{4} r_i exp(\lambda_i t) \end{matrix}. \tag{7}$$

2. Unstable Flight

Eq. 6 suggests defining a discriminant δ of flight stability with

$$\delta = \frac{1}{\bar{P}_L}[(a-d)^2 + 4bc] = \left[\frac{b_i^{(m)}}{m} - \frac{b_{\vartheta,i}^{(L)}}{J}\right]^2 + 4\frac{b_{\vartheta,i}^{(m)}}{m}\frac{b_i^{(L)}}{J}. \tag{8}$$

With $\delta < 0$, $\mu_{1,2}$ becomes complex and, as shown in greater detail in [16], for any initial conditions $r(0) = r_0,\ \vartheta(0) = \vartheta_0,\ \dot{r}(0) = \dot{\vartheta}(0) = 0$ the lateral and angular motion can be described by

$$\begin{pmatrix} r(t) \\ \vartheta(t) \end{pmatrix} = exp(\kappa t) \begin{pmatrix} \hat{r}\, cos(\omega t + \varphi) \\ \hat{\vartheta}\, cos(\omega t + \varphi + \Delta\varphi) \end{pmatrix}. \quad (9)$$

Here,

$$\omega = \frac{\bar{P}_L}{4} \frac{\sqrt{-\delta}}{\kappa} > 0 \quad (10)$$

represents the oscillatory character of lateral and angular motion with respect to the beam center and orientation, resp.

$$\varphi = tan^{-1} \left[cot\, \Delta\varphi - \frac{\vartheta_0}{r_0 \cdot \varrho \cdot sin\Delta\varphi} \right] \quad (11)$$

with

$$\varrho = \frac{\sqrt{ad-bc}}{b} \quad (12)$$

takes into account for the initial conditions at $t = 0$ and

$$\Delta\varphi = tan^{-1} \frac{\sqrt{-(a-d)^2-4bc}}{a+d} \quad (13)$$

yields a phase shift between lateral and angular oscillation. However, the positive parameter κ with

$$\kappa = \frac{1}{2} \sqrt{\bar{P}_L \left[\frac{b_i^{(m)}}{m} + \frac{b_{\vartheta,i}^{(L)}}{J} + \sqrt{\left[\frac{b_i^{(m)}}{m} + \frac{b_{\vartheta,i}^{(L)}}{J} \right]^2 - \delta} \right]} > 0 \quad (14)$$

indicates the divergent character of lateral and angular motion, cf. Eq. 8. In other words:

A BEP craft with a flight dynamics matrix yielding $\delta < 0$ is not expected to ride the laser-beam.

3. Beam-Riding

However, $\delta \geq 0$ is only a necessary criterion for beam-riding stability, but not a sufficient one, since the destabilizing expression $\exp(\kappa t)$ with $\kappa > 0$, cf. Eq. 9, still can occur in the equations of motion when $\mu_{1,2} > 0$.

Only when λ becomes imaginary, i.e. $\mu_{1,2} < 0$, an oscillatory motion around the beam center and the beam direction, resp., can be achieved where the corresponding amplitude does not diverge. This is the case for $\mu_1 < 0$ yielding the sufficient condition $\varepsilon \leq 0$ for beam-riding with

$$\varepsilon = \frac{1}{\bar{P}_L}\left[a + d + \sqrt{(a-d)^2 + 4bc}\right]$$

$$= \left[\frac{b_i^{(m)}}{m} + \frac{b_{\vartheta,i}^{(L)}}{J} + \sqrt{\left[\frac{b_i^{(m)}}{m} - \frac{b_{\vartheta,i}^{(L)}}{J}\right]^2 + 4\frac{b_{\vartheta,i}^{(m)}}{m}\frac{b_i^{(L)}}{J}}\right], \qquad (15)$$

provided $\delta \geq 0$, as mentioned above. Hence,

$$\frac{b_i^{(m)}}{m} + \frac{b_{\vartheta,i}^{(L)}}{J} \leq -\sqrt{\left(\frac{b_i^{(m)}}{m} - \frac{b_{\vartheta,i}^{(L)}}{J}\right)^2 + \frac{b_{\vartheta,i}^{(m)}}{m}\frac{b_i^{(L)}}{J}}, \qquad (16)$$

is the sufficient criterion for beam-riding which, roughly spoken, is fulfilled, when back-driving forces and momenta, represented by negative values of $b_i^{(m)}$ and $b_{\vartheta,i}^{(L)}$ on the left hand side of Eq. 16, dominate the coupling of lateral and angular motion, represented mainly by $b_{\vartheta,i}^{(m)}$ and $b_i^{(L)}$ on its right hand side.

3. EXAMPLE: PARABOLIC LASER LIGHTCRAFT

Laser propulsion experiments have been carried out at DLR Stuttgart with an air-breathing parabolic thruster made of aluminum. A metallic ignition pin was implemented on its axis of symmetry in order to provide for reproducible laser-induced air breakdown at the focus and to prevent off-axis detonation [17]. Offset and inclination against the laser beam center and propagation axis, resp., however, yield an inhomogeneous intensity distribution on the ignition pin surface and, during the temporal course of the laser pulse, inside the expanding laser-induced plasma [18]. The occurrence of lateral and rotational impulse components can be ascribed to these phenomena, cf. as well similar work on the LTD engine [19,20,21].

In [14], we reported on a hovering experiment with a parabolic laser lightcraft where, after an initial launch sequence, the average laser power was adapted to the craft's mass in order to analyze its beam-riding stability. Supplementary experimental data and analyses were carried out in [16] and are summarized in the following.

A. Trajectories

Trajectory analysis was carried out using 500 fps video data from a high speed camera. The lightcraft's motion was recorded in a stereoscopic view of 4 tracking markers on each side of the lightcraft's protective shell enabling the reconstruction of center-of-mass position and angular orientation [12,13].

1. Experimental results

More than 80 hovering flight experiments were carried out at the CO_2 high energy laser of DLR Stuttgart with an average laser pulse energy $\bar{E}_L \approx 110$ J. The lightcraft's mass amounted around 70 g yielding a laser repetition rate $f_{rep} \approx 25$ Hz for hovering at a constant altitude of approx. 6 cm. Though the lightcraft was thoroughly aligned to the laser beam propagation axis and lateral offset to beam center was minimized and, later on, systematically varied up to several millimeters, resp., the lightcraft failed to exhibit a quasi-stable state of dynamic equilibrium in a hovering flight for longer than 8 pulses, i.e. 0.32 seconds. Instead, lateral offset and inclination angle increased from approximately zero to significant high values in an oscillatory way, as shown for an experimental subset (A in [14,16]) of around 30 flights in Fig. 1.

In order to understand this flight behavior, momentum coupling was investigated for each laser pulse depending on lateral offset and inclination angle. Therefore, for each laser pulse, a momentary plane of inclination of the lightcraft was determined, denoted by the subscript s in the following, whereas the subscript *k* refers to the perpendicular plane where no inclination angle appears. Then, linear approximation of impulse coupling datasets following

$$\begin{pmatrix} c_{m,s} \\ c_{L,s} \\ c_{m,k} \\ c_{L,k} \end{pmatrix} \approx \begin{pmatrix} b_\vartheta^{(m,s)} & b_s^{(m,s)} & b_k^{(m,s)} \\ b_\vartheta^{(L,s)} & b_s^{(L,s)} & b_k^{(L,s)} \\ b_\vartheta^{(m,k)} & b_s^{(m,k)} & b_k^{(m,k)} \\ b_\vartheta^{(L,k)} & b_s^{(L,k)} & b_k^{(L,k)} \end{pmatrix} \begin{pmatrix} \vartheta \\ r_s \\ r_k \end{pmatrix} \tag{17}$$

was performed. However, the limited range of the backdriving forces and momenta was taken into account using an approximation term which was modified by Lorentz functions in the denominator, given by

$$\frac{b_\vartheta \cdot \vartheta + b_s \cdot r_s + b_k \cdot r_k}{\left[1+\left[\frac{\vartheta}{\sigma_\vartheta}\right]^2\right] \cdot \left[1+\left[\frac{r_s}{\sigma_s}\right]^2\right] \cdot \left[1+\left[\frac{r_k}{\sigma_k}\right]^2\right]}. \tag{18}$$

From the corresponding datafits it was found that momentum coupling in the *s*-plane is nearly independent from r_k and, vice versa, r_s and ϑ do almost not affect momentum coupling in the *k*-plane. Hence, Eq. 17 reduces to

$$\begin{pmatrix} c_{m,s} \\ c_{L,s} \end{pmatrix} = \begin{pmatrix} -2\ N/(MW \cdot deg) & -0.4\ N/(MW \cdot mm) \\ -70\ mN \cdot m/(MW \cdot deg) & +20\ mN \cdot m/(MW \cdot mm) \end{pmatrix} \begin{pmatrix} \vartheta \\ r_s \end{pmatrix} \tag{19}$$

and

$$\begin{pmatrix} c_{m,k} \\ c_{L,k} \end{pmatrix} = \begin{pmatrix} -0.4\ N/(MW \cdot mm) \\ +40\ mN \cdot m/(MW \cdot mm) \end{pmatrix} r_k \tag{20}$$

with the corresponding approximate results according to the fits of experimental data.

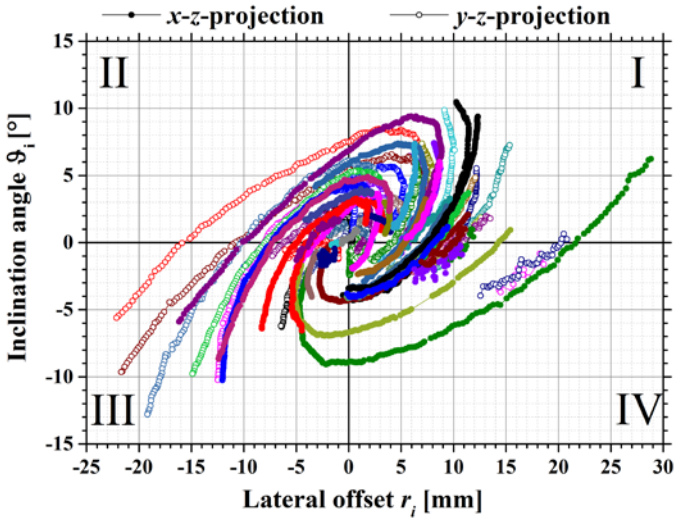

FIGURE 1. Flight trajectories $\vartheta_x(r_x)$ and $\vartheta_y(r_y)$ for the hovering sequences of several free flights of a parabolic lightcraft. The motion through the quadrants reads as follows: I. The craft is on the right hand side of the beam and points to the beam center. II. The craft has crossed the beam center and points away from the beam. III. The craft is still on the left hand side of the beam but now points towards the beam center again. IV. Having crossed the beam center again, the lightcraft is back on the right hand side of the beam and points away from the beam center.

The results given in Eq. 19 allow for an interpretation of the flight trajectories which are depicted in Fig. 1:

In the first quadrant (I), back-driving lateral impulse components occur which are enhanced by the inclination of the lightcraft towards the beam center, $b_{\vartheta,i}^{(m,i)}<0,\ \vartheta>0$. In the second quadrant, however, the latter dependency, $c_{m,i}(\vartheta_i)$, yields a repulsive momentum component capable to compensate the back-driving lateral impulse component given by $b_i^{(m,i)} < 0$. With the transition from III to IV, occurrence and fade-out of back-driving lateral impulse can be seen again. Hence, it can be pointed out that experimental analysis revealing $b_i^{(m,i)} < 0$ does not present a sufficient criterion for beam-riding, but the interdependency of lateral and angular motion plays an important role as well.

Similar findings can be stated for the angular motion where the lateral offset provides for enhancement (II, IV) or reduction (I,III), resp., of back-driving angular momentum.

2. Simulation results

The fitting results from Eq. 19 allow for characterization of the lightcraft's motion according to the flight dynamics matrix theory, as sketched above. The corresponding figures of merit are given in Table 1. It can be seen that $\delta < 0$ indicates the failure of beam-riding flights. The result for the oscillation period T of lateral and angular

motion, cf. [18] for a more detailed description in a different experiment, matches the experimental findings quite well. However, the positive value of the damping constant κ demonstrates the fast increase of the corresponding amplitudes yielding the spiraled trajectories depicted in Fig. 1.

TABLE 1. Analytical results from flight dynamics matrix theory for the motion of a parabolic lightcraft in the plane of inclination with $\overline{P}_L \approx 2.75\ kW, m \approx 70\ g, J \approx 0.1\ g \cdot m^2$.

Figure of merit	Result
Beam-riding discriminant δ	$-1.27 \cdot 10^{-4}\ J^{-2}s^{-2}$
Oscillation period T	$0.78\ s$
Damping constant κ	$0.97\ s^{-1}$

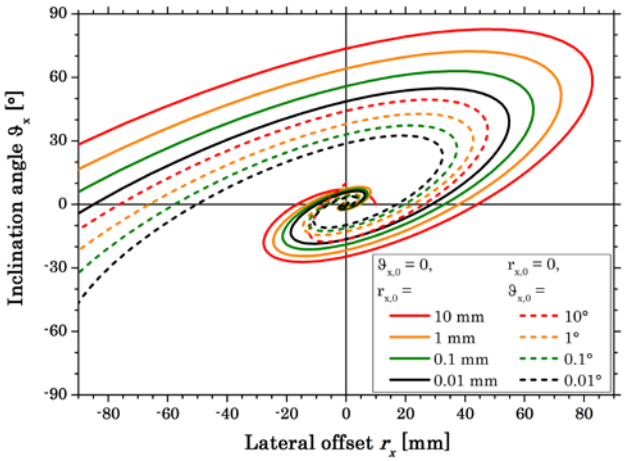

FIGURE 2. Simulation of trajectories based on experimental data of momentum coupling for different initial conditions at launch.

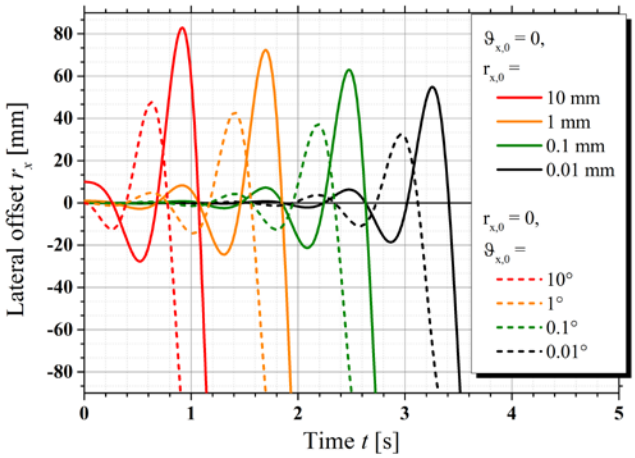

FIGURE 3. Simulation of the temporal course of lateral offset based on experimental data of momentum coupling for different initial conditions at launch.

In reality, however, the plane of inclination changes from laser pulse to pulse. The reason can be found in Eq. 20 showing that a lateral offset perpendicular to the momentary plane of inclination induces angular momentum being perpendicular to this plane as well yielding a rotation of the plane of inclination which has already been

observed in [14]. Hence, reduction of the lightcraft's motion to the momentary plane of inclination is only suitable as a first 2D approach for flight dynamics analysis.

Therefore, in a way similar to Eq. 18, the experimental data of subset A were fitted according to

$$\frac{b_{\vartheta,x}\cdot\vartheta_x+b_x\cdot r_x+b_{\vartheta,y}\cdot\vartheta_y+b_y\cdot r_y}{\left[1+\left[\frac{\vartheta_x}{\sigma_{\vartheta,x}}\right]^2\right]\cdot\left[1+\left[\frac{r_x}{\sigma_x}\right]^2\right]\cdot\left[1+\left[\frac{\vartheta_y}{\sigma_{\vartheta,y}}\right]^2\right]\cdot\left[1+\left[\frac{r_y}{\sigma_y}\right]^2\right]} \tag{21}$$

as shown in detail in [16]. Note that, in contrast to the definition of ϑ in Eq. 17, ϑ_x and ϑ_y denote the projection of ϑ in the *x*-*z* and *y*-*z* plane, resp., with $\tan^2\vartheta = \tan^2\vartheta_x + \tan^2\vartheta_y$. In [16], it has been found that the motions in both planes are not completely independent from each other. However, as a first approach, this can be neglected since dependencies of the motion in one plane from angle and position in the other plane are around one magnitude smaller than the corresponding dependencies within the same plane.

With this simplification the results from the datafits in the *x*-*z* plane were inserted into Eq. 3 yielding the spiraled trajectories depicted in Fig. 2. They exhibit the same characteristic shape as the trajectories from the experiment in shown Fig. 1. In spite of all simplifications, this demonstrates the suitability of Eq. 3 to describe the lightcraft's motion.

B. Discussion

Complementarily to experimental data, simulation results allow for an extended discussion of relevant parameters affecting the beam-riding abilities of a laser lightcraft.

1. Alignment accuracy

As it can be seen from experimental data, cf. Fig. 1, and the corresponding simulation results, cf. Fig. 2, beam-riding is not achieved in the examined setup. Moreover, Fig. 2 indicates that alignment accuracy seems not to be the crucial issue for beam-riding in this experiment, in contrast to our first assumptions. In fact, $\delta < 0$ was found for all hovering experiments indicating the impossibility of beam-riding in this particular experimental setup. Simulations allow for a virtual variation of alignment accuracy at the launch position. As depicted in Fig. 3 for initial offset and initial inclination angle separately, improvement of alignment accuracy by one order of magnitude yields an increased time of laser-powered flight of less than one second until the lightcraft drops off the beam. Hence, beam-riding ability has to be addressed systematically by the engine's parameters.

2. Center-of-mass position

Whereas in the experiments only the parabolic engine itself was examined, transportation of a payload has to be investigated as well with respect to beam-riding. This does not only imply a change of m and J. In fact, since the position of the system's center-of-mass changes, the apportionment of the total imparted impulse into lateral and rotational components changes significantly yielding a modification of the coefficients $b_l^{(k)}$ of the craft-specific matrix of flight dynamics. A corresponding detailed vector analysis is given in [16].

Fig. 4 depicts the changes in the coefficients $b_l^{(k)}$ for a wide range of payload masses. When the center mass is lifted into the upper half of the thruster, coupling dependencies change significantly due to sign changes of the impulse components. Moreover, the dependency of both lateral and angular momentum on the inclination angle of the craft gets more pronounced. In this range, $\delta > 0$, i.e. the necessary criterion for beam-riding is fulfilled, however, since $\varepsilon > 0$, the sufficient condition is not met. Namely, at $z_{CMS} = 65$ mm, $\varepsilon < 0$ is found and theoretically, beam-riding is achieved, cf. Fig. 5 . However, the corresponding error bar of ε ranges far towards positive values, hence it is doubtful if a real engine in this configuration would ride the laser beam.

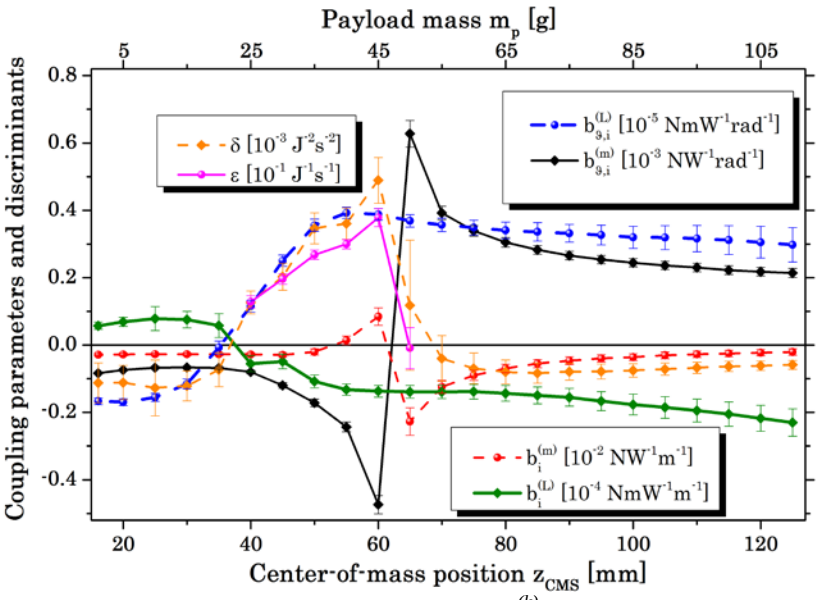

FIGURE 4. Payload study: Dependency of the coefficients $b_l^{(k)}$ of the craft-specific matrix of flight dynamics and beam-riding criteria δ, ε on payload mass and center-of-mass position. The lightcrafts aperture is located at z = 0 mm, its apex at z = 62.5 mm. The payload is represented by an aluminium cylinder of 16 to 22 mm diameter placed above the thruster on a platform at z = 70 mm.

3. Pulsed motion

In our analytical approximation of Eq. 3 we introduced a quasi-continuous approach of the lightcraft's motion which, in fact, is a pulsed one. A more detailed simulation can be carried out, if the trajectory is calculated piecewise with ballistic

segments from pulse to pulse whereas $c_{m,i}(x, y, z, \vartheta_x, \vartheta_y)$ and $c_{L,i}(x, y, z, \vartheta_x, \vartheta_y)$ are evaluated for each laser pulse time t_p. This can be carried out for various initial values of inclination ϑ_0 and offset r_0 at the launch position yielding the corresponding maximum flight duration and the achieved maximum altitude compared with perfect alignment ($\vartheta_0 = r_0 = 0$). The set of launch parameters which yield beam-riding stability is somehow comparable with a Julia set, and hence this method shows some similarities with the computation of fractals, cf. [16,18] for further details.

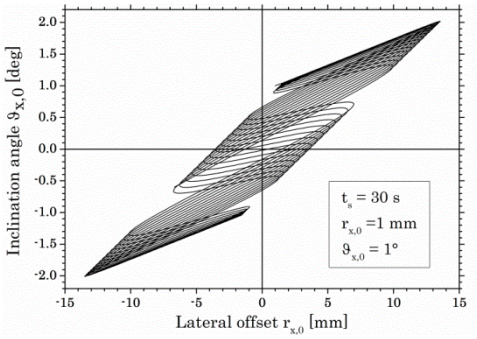

FIGURE 5. Simulated trajectories for a theoretical beam-riding configuration with $\varepsilon < 0$.

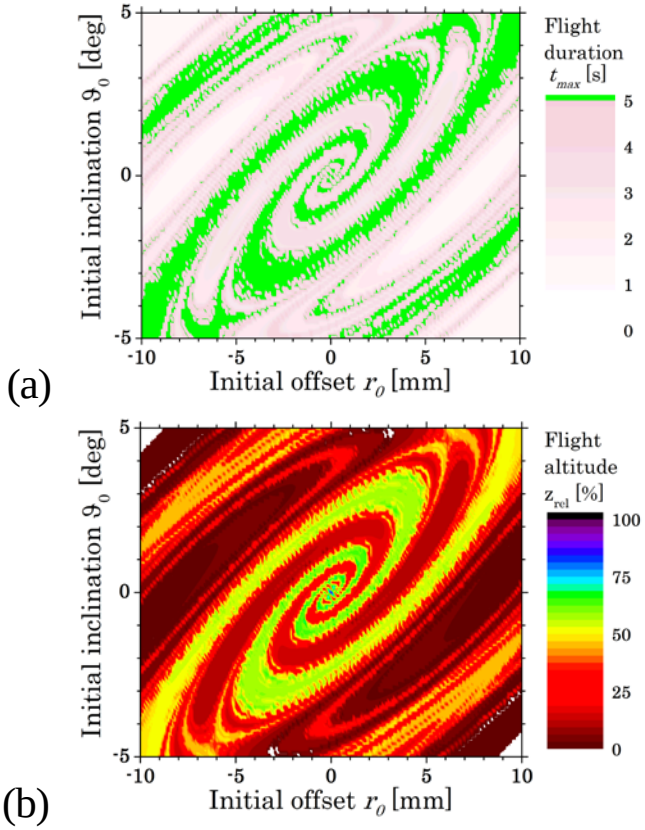

FIGURE 6. (a) Simulated maximum flight duration and (b) maximum flight altitude of a parabolic laser lightcraft powered with $\overline{P}_L$ = 5 kW, E_L = 100 J, and f_{rep} = 50 Hz. Simulation time t_s = 5 s, i.e., parameter sets yielding a flight that is not finished after $\boldsymbol{t_s}$ (green in the upper graph), do not automatically imply beam-riding, but might result in later beam drop-off which was not calculated due the limitation of $\boldsymbol{t_s}$.

Fig. 6 depicts the corresponding results for the parabolic laser lightcraft. However, in contrast to the hovering experiments with $\bar{P}_L \approx 2.75$ kW, an increased average laser power $\bar{P}_L = 5$ kW was used to examine the lightcraft's lift-off. Moreover, the dependency of $c_{m,z}$ from offset and inclination, as already reported in [14], allows for a determination of the point in time when craft drops off the beam. The really surprising result is shown in Fig. 6(a): From our quasi-continuous simulations on hovering experiments, we would expect that an increase of alignment accuracy would result in a longer flight time. Taking pulsed motion into account, we see that this is not the case. Instead, the variation of alignment accuracy at launch exhibits a butterfly effect with respect to the flight time and altitude which is highly critical for the thruster configuration itself.

4. CONCLUSIONS

The concept of a craft-specific matrix of flight dynamics has been applied to a parabolic laser lightcraft as an example for any beamed-energy propelled vehicle. Though the matrix concept represents a 2D and continuous simplification of the 3D pulsed motion, a good agreement between experimental and simulated trajectories was found. Failure of beam-riding, as stated in the experiments, can be deduced from corresponding beam-riding criteria in connection with coupling between lateral and angular motion. Alignment accuracy at launch plays a minor role here, especially since a butterfly effect was detected in pulsed motion simulation. With respect to beamed-energy propulsion system design, overall mass, momentum of and inertia and center-of-mass position can change momentum coupling properties and beam-riding abilities significantly.

In the following, some options to achieve beam-riding shall be sketched.

1. Geometric optimization

The usage of a metallic ignition pin on the lightcraft's axis of symmetry provides for detonation on the symmetry axis and contributes to flight stability as shown in [12,13]. Nevertheless, in the case of lateral offset and/or inclination of the craft, the fluence distribution Φ on the pin shows a great dependency on the azimuthal angle $\tilde{\varphi}$ inside the lightcraft yielding different initial conditions for laser-induced detonation in the various spatial segments of the craft. Though corresponding raytracing simulations are only a first step to analyze the complex problem of non-symmetric detonation, interrelations of fluence distributions and impulse coupling fields $c_{m,i}(r_j, \vartheta_k)$ and $c_{L,i}(r_j, \vartheta_k)$ can be seen clearly [16,18]. For a more detailed study, finite-element methods have to be applied [21] which should take laser-matter interaction during the laser pulse into account [19].

In the parabolic lightcraft, as well as in Myrabo's LTD, the focusing geometry acts an expansion nozzle. This twofold role is the background for the strong dependency of the fluence distribution in the focal area and the resulting impulse coupling fields on

the craft's attitude. Thorough simulations on detonation dynamics might allow for geometric optimization of the focusing nozzle towards beam-riding abilities.

Optimizations might concern length and diameter of the focusing nozzle, but considerations of the whole geometry shape and configuration as well: Fig. 7 depicts the concept of a honeycomb-like thruster array, as already proposed in [22]. The knowledge of the angular dependency of the lateral coupling coefficient allows for optimization of overall lateral coupling by optimum inclination of the outer six nozzles. Beam-stability with respect to angular motion, however, is not addressed with this concept and therefore has to be granted by spin-stabilization.

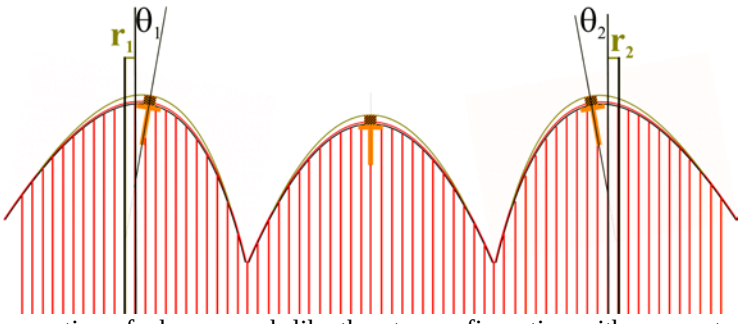

FIGURE 7. Cross-section of a honeycomb-like thruster configuration with one central and six outer parabolic thrusters [16]: For coaxial alignment of the whole craft on the laser beam, the outer nozzles experience a lateral offset of $r = \pm 10$ mm and an inclination of $\vartheta = \pm 10°$ which results in enhanced restoring lateral impulse components.

2. Movable detonation center

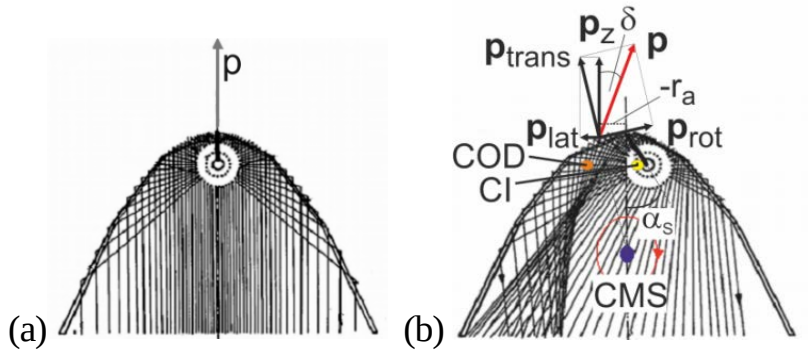

FIGURE 8. Scheme of the imparted impulse inside a parabolic laser lightcraft (a) with an ignition pin on the axis of symmetry and (b) with a tilted ignition pin as a steering device, cf. [17,23]. In both cases, the lightcraft is aligned coaxially to the laser beam. The propagation of the laser-induced shockwaves inside the craft indicates coaxial momentum transfer for perfect alignment with an ignition pin on the symmetry axis. Inclination of the ignition device by the angle $\boldsymbol{\alpha_S}$, however, yields a shift of the center of intensity (CI) on the pin, raising lateral and rotational momentum.

The ignition pin inside the parabolic lightcraft was not only intended for detonation reproducibility but for steering issues as well [17]. The pin can be tilted against the symmetry axis of the craft which results in a modified fluence distribution on the pin yielding a shift of the detonation center (COD) inside the craft together with a modification of the imparted momentum, cf. Fig. 8. However, though the thrust vector can be altered and inclined by the thrust angle δ in this way, even in a thorough

analysis of the corresponding impulse coupling fields $c_{m,i}(r_j, \vartheta_k, \alpha_S)$ and $c_{L,i}(r_j, \vartheta_k, \alpha_S)$, no suitable steering sequence for beam-riding has been found yet [16]. Lateral impulse coupling can be optimized, but this is limited to the plane of inclination of the ignition pin.

In general, a dynamic feedback loop from lightcraft attitude to focus positioning might help to achieve beam-riding and steering for orbit insertion.

3. Optical decoupling

Beam-riding optimizations on the focusing nozzle geometry with respect to mass, momentum of inertia and the center of mass position might be cumbersome. As an alternative, decoupling of the focusing optics from the nozzle geometry can be undertaken. This approach is realized in the Russian demonstrator ASLPE (Aerospace Laser Propulsion Engine). In this concept, the incoming laser light is focused by a combination of an inverted parabolic mirror and a parabolic ring segment of which the latter one directs the focused beam into the center of a conical nozzle [24]. Hence, the impulse receiving nozzle is not used as a focusing optics which should minimize performance changes due to the craft's attitude and the resulting inhomogeneity of the fluence distribution. However, to the author's knowledge, impulse coupling fields have not been analysed for the ASLPE yet.

4. Spin-stabilization

If the angular motion of the lightcraft is suppressed by means of spin-stabilization, beam-riding reduces to the question of lateral restoring impulses and, in the later course of the flight, of a stable flight under increasing inclination between the laser-beam and the craft in higher altitudes on its way to orbit insertion. In that case, optimization of the lightcraft geometry might be easier, but controllability and perhaps de-spinning of the rotating lightcraft has to be assured which might require additional structural mass onboard the laser-propelled system.

5. Beam positioning

In [25,26], Takahashi and Ohnishi proposed an elegant method to overcome insufficient lateral restoring forces, namely by an adaptation of the laser-beam position to the craft's attitude. Roughly speaking, the laser beam moves around the lightcraft in order to compensate the craft's insufficient ability of stable oscillations around the laser beam center. Only the lateral offset of the craft but not its inclination is addressed by this concept. Therefore, it might work out well if any disturbing angular motion is suppressed by spin-stabilization. However, a feedback loop between attitude analysis and laser beam positioning has to be installed.

Especially the latter option of beam positioning highlights the strong requirements for beam-riding on pointing and tracking of the remotely propelled object, which is expected to be crucial for any beam-riding purposes.

REFERENCES

1. A. Kantrowitz, "Propulsion to Orbit by Ground-Based Lasers", *Astronautics and Aeronautics* **10**(5), pp. 74–76, 1972.
2. W. Schall and H.-A. Eckel, "Pulsed Laser Propulsion Experiments", *Space Technology* **24**, pp. 129–135, 2004.
3. W.L. Bohn, "Laser Propulsion – Quo vadis", *AIP Conf. Proc.* **997**, pp. 47–55, 2008.
4. S. Scharring, H.-A. Eckel, J. Trommer, H.-P. Röser, and C. Eigenbrod, „Spaceborne Lightcraft Applications – an Experimental Approach", *AIP Conf. Proc.* **997**, pp. 295–303, 2008.
5. Yu. Rezunkov and A.V. Pakhomov, "Perspective In-Space Laser Propulsion Demonstrator Mission", *AIP Conf. Proc.* **702**, pp. 205–215, 2004.
6. L.N. Myrabo, "World Record Flights of Beam-Riding Rocket Lightcraft: Demonstration of 'Disruptive' Propulsion Technology", AIAA paper 2001-3798.
7. L. Myrabo and D. Ing, "The Future of Flight", Bean Enterprises, New York, 1985, cited in [6].
8. M.A. Libeau, L.N. Myrabo, M. Filippelli, and J. McInerney, "Combined Theoretical and Experimental Flight Dynamics Investigation of a Laser-Propelled Vehicle", *AIP Conf. Proc.* **664**, pp. 125–137, 2003.
9. M. Libeau, and L.N. Myrabo, "Off-Axis and Angular Impulse Measurements on a Lightcraft Engine", *AIP Conf. Proc.* **766**, pp. 166–177, 2005.
10. D.A. Kenoyer, K.S. Anderson, and L.N. Myrabo, "Calibration and Validation of a 6-DOF Laser Propelled Lightcraft Flight Dynamics Model vs. Experimental Data", *AIP Conf. Proc.* **997**, pp. 325–337, 2008.
11. D.A. Kenoyer, I.I. Salvador, and L.N. Myrabo, "Beam-Riding Behavior of Lightcraft Engines with ≈ 1 μs Pulsed TEA CO_2 Laser, *AIP Conf. Proc.* **1402,** pp. 93–105, 2011.
12. S. Scharring, D. Hoffmann, H.-A. Eckel, and H.-P. Röser, "Stabilization and steering of a parabolic laser thermal thruster with an ignition device", *Acta Astronautica* **65**, pp. 1599–1615, 2009.
13. S. Scharring, H.-A. Eckel, and H.-P. Röser, "High speed analysis of free flights with a parabolic thruster", *AIP Conf. Proc.* **1230,** pp. 77–88, 2010.
14. S. Scharring, H.-A. Eckel, and H.-P. Röser, "Beam-Riding Analysis of a Parabolic Laser-Thermal Thruster", *AIP Conf. Proc.* **1402,** pp. 115–131, 2011.
15. I.N. Bronstein, K.A. Semendjajew, G. Musiol, and H. Mühlig, Taschenbuch der Mathematik, 2. ed, publisher: Verlag Harry Deutsch, Frankfurt (Main), Germany, 1995, (in German)
16. S. Scharring, Impulse analysis of air-breathing pulsed laser-thermal propulsion with a parabolic reflecting nozzle for space applications, PhD thesis, University of Stuttgart, 2013 (in German), http://elib.uni-stuttgart.de/opus/volltexte/2013/8360/
17. W.O. Schall, E. Zeyfang, W. Riede, and W. Mayerhofer, "Propulsion device and method of generating shock waves", Patent DE 100 17 343 C2, filed 7 April 2000 (in German) and US 2002/0047673 A1, filed 6 April 2001.
18. S. Scharring, H.-A. Eckel, and H.-P. Röser, Beam-Riding of a Parabolic Laser Lightcraft, *International Journal of Aerospace Innovations* **3**(1), pp. 15–31, 2011.
19. T.-S. Wang, Y.-S. Chen, J. Liu, L.N. Myrabo, and F.B. Mead Jr., "Advanced Performance Modeling of Experimental Laser Lightcraft", *J. Prop. Pow.* **18**, pp. 1129–1138, 2002.
20. D.A. Kenoyer, I.I. Salvador, S.N. Notaro, and L.N. Myrabo, "Flow Visualization of Thrust-Vectoring Lightcraft Engines with ~1μs Pulsed TEA CO_2 Laser", *AIP Conf. Proc.* **1402**, pp. 106–114, 2011
21. M. Takahashi and N. Ohnishi, "Three-Dimensional Numerical Analysis for Posture Stability of Laser Propulsion Vehicle", *AIP Conf. Proc.* **1402**, pp. 132–141, 2011
22. W. Schall, "Lightcraft – Tasks", *unpublished conceptional considerations*, DLR Stuttgart, 2005.
23. S. Scharring, D. Hoffmann, H.-A. Eckel, and H.-P. Röser, "Remotely Controlled Steering Gear for a Laser-driven Rocket with a Parabolic Thruster", *AIP Conf. Proc.* **1230,** pp. 89–100, 2010.
24. A.A. Ageichik, M.S. Egorov, Y.A. Rezunkov, A.L. Safronov, V.V. Stepanov, "Experimental Study on Thrust Characteristics of Airspace Laser Propulsion Engine", *AIP Conf. Proc.* **702**, pp. 49–60, 2004.
25. M. Takahashi, and N. Ohnishi, "Beam Riding Performance of Asymmetrically Propelled Laser Vehicle", *AIAA Journal* **50**(11), pp. 2600–2608, 2011.
26. M. Takahashi, and N. Ohnishi, "Performance Analysis of Beam Riding Vehicle with Motion Synchronized Laser Pulse", AIAA paper 2012-3302.